© 2019. Published by The Company of Biologists Ltd | Journal of Cell Science (2020) 133, jcs232991. doi:10.1242/jcs.232991

RESEARCH ARTICLE

SPECIAL ISSUE: CELL BIOLOGY OF THE IMMUNE SYSTEM

Differential nanoscale organisation of LFA-1 modulates T-cell migration

Michael J. Shannon[1,‡], Judith Pineau[1], Juliette Griffié[1], Jesse Aaron[2], Tamlyn Peel[3], David J. Williamson[1], Rose Zamoyska[4], Andrew P. Cope[3,*], Georgina H. Cornish[3,*] and Dylan M. Owen[1,5,*,‡]

ABSTRACT

Effector T-cells rely on integrins to drive adhesion and migration to facilitate their immune function. The heterodimeric transmembrane integrin LFA-1 (αLβ2 integrin) regulates adhesion and migration of effector T-cells through linkage of the extracellular matrix with the intracellular actin treadmill machinery. Here, we quantified the velocity and direction of F-actin flow in migrating T-cells alongside single-molecule localisation of transmembrane and intracellular LFA-1. Results showed that actin retrograde flow positively correlated and immobile actin negatively correlated with T-cell velocity. Plasma membrane-localised LFA-1 forms unique nano-clustering patterns in the leading edge, compared to the mid-focal zone, of migrating T-cells. Deleting the cytosolic phosphatase PTPN22, loss-of-function mutations of which have been linked to autoimmune disease, increased T-cell velocity, and leading-edge co-clustering of pY397 FAK, pY416 Src family kinases and LFA-1. These data suggest that differential nanoclustering patterns of LFA-1 in migrating T-cells may instruct intracellular signalling. Our data presents a paradigm where T-cells modulate the nanoscale organisation of adhesion and signalling molecules to fine tune their migration speed, with implications for the regulation of immune and inflammatory responses.

This article has an associated First Person interview with the first author of the paper.

KEY WORDS: Integrins, LFA-1, T-cell migration, SMLM, dSTORM

INTRODUCTION

The heterodimeric integrin lymphocyte functional antigen-1 (LFA-1; αLβ2 integrin) is a transmembrane heterodimer highly expressed on T-cells. It is essential for T-cell function and is required for naïve lymphocyte antigenic activation, recruitment of immune cells to sites of infection and cytotoxic killing. LFA-1 expressed on effector T-cells binds to intracellular adhesion molecule (ICAM)-1 to induce rapid migration *in vivo* and *in vitro* (Hons et al., 2018; Teijeira et al., 2017). The force required for migration is generated by actin polymerisation and myosin-driven actin flow, and integrin adhesion molecules on the cell surface, which couple the actin flow to the underlying substrate (Shannon et al., 2015). Actin and integrins are indirectly linked via a group of proteins collectively known as the molecular clutch, which regulates this mechanical coupling (Ishibashi et al., 2015; Chen et al., 2012; Case and Waterman, 2015). The control of this linkage is integral to achieving high-speed migration (Hons et al., 2018) and is especially important during inflammation (Teijeira et al., 2017). It is also known that integrins can exist in low, intermediate and high affinity states that describe a specific pattern of localisation within migrating T-cells. Low and intermediate affinity integrin molecules are located in the leading edge (LE), whereas high affinity LFA-1 is located in the mid cell body (focal zone; FZ) (Smith et al., 2005).

Control of adhesion is achieved through actin linkers (talin and vinculin) and regulatory kinases [FAK (also known as PTK2) and Src family kinases] (Nordenfelt et al., 2016; Raab et al., 2017), a mechanism originally described in other, much more slowly migrating cell types that characteristically form large micron sized focal adhesions (Kanchanawong et al., 2010). These components were originally described in slow migrating adherent cells that characteristically form large micron-sized focal adhesions (Kanchanawong et al., 2010). In T-cells, these complexes are small (nanoscale) (Burn et al., 2016), similar in size and composition to nascent adhesions (Changede et al., 2015), and their spatial organisation may represent a novel paradigm for the nanoscale regulation of adhesion and migration.

Conventional fluorescence microscopy is limited in resolution to ∼200 nm. Recently, a number of super-resolution approaches have been developed to overcome this limitation. Single-molecule localisation microscopy (SMLM), here implemented as stochastic optical reconstruction microscopy (STORM) (Rust et al., 2006), utilises fluorophore dark-states and sequential imaging to generate lists of molecular coordinates with a mean of 10 nm precision in fixed cells. By using Bayesian statistical cluster analysis (Griffié et al., 2016; Rubin-Delanchy et al., 2015), it is possible to accurately quantify protein clustering at the nanoscale. This includes clustering of intracellular molecular populations via 3D interferometric SMLM imaging featuring isotropic resolution (Shtengel et al., 2009; Griffié et al., 2017). Such populations of intracellular, membrane proximal LFA-1 and FAK may represent distinct nanoscale arrangements recruited to form new adhesions in the membrane.

Here, we investigated the dynamics of retrograde actin flow alongside the nanoscale organisation of actively signalling LFA-1 nanoclusters in primary murine T blasts migrating on ICAM-1-coated coverslips. A range of conditions were used to modulate cell speed including addition of Mn^{2+} (which push integrins into the high affinity state; Dransfield et al., 1992), high density ligand (to increase adhesion), the addition of the chemokine CXCL12 (to induce signalling through CXCR4) and cytochalasin D (CytoD,

[1]Department of Physics and Randall Centre for Cell and Molecular Biophysics, King's College London, London WC2R 2LS, UK. [2]Advanced Imaging Center, HHMI Janelia Research Campus, Ashburn, VA 20147, USA. [3]Centre for Inflammation Biology and Cancer Immunology, School of Immunology and Microbiological Sciences, King's College London, London SE1 1UL, UK. [4]School of Biological Sciences, University of Edinburgh, Edinburgh EH9 3FL, UK. [5]Institute of Immunology and Immunotherapy and Department of Mathematics and Centre for Membrane Proteins and Receptors (COMPARE), University of Birmingham, Birmingham B15 2TQ, UK.
*These authors contributed equally to this work

‡Authors for correspondence (d.owen@bham.ac.uk; mjs2399@cumc.columbia.edu)

T.P., 0000-0003-4188-612X; D.J.W., 0000-0002-6222-6297; D.M.O., 0000-0002-5284-2782

Received 8 April 2019; Accepted 21 August 2019

Journal of Cell Science (2020) 133, jcs232991. doi:10.1242/jcs.232991

which inhibits actin polymerisation; Goddette and Frieden, 1986). We then included in our analysis cells lacking the phosphatase PTPN22, a negative regulator of migration (Burn et al., 2016) where a loss-of-function mutation (Svensson et al., 2011) causes a rapid migration phenotype in T-cells and predisposes humans and mice to a range of autoimmune diseases (Dai et al., 2013; Burn et al., 2011; Brand et al., 2005; Bottini et al., 2006; Begovich et al., 2004). By characterising the nanoclustering of LFA-1 and its regulators as a previously un-investigated aspect of the molecular clutch model, we are able to link changes in their membrane and submembrane arrangement to the functional output of cell speed and actin flow/engagement changes during rapid polarised migration.

RESULTS

The speed of actin retrograde flow is positively correlated with T-cell velocity and negatively correlated with immobile actin

Inside-out and outside-in activation of LFA-1 regulates its affinity maturation and translates into functional effects on adhesion and migration behaviour. Filamentous actin (F-actin) forms networks of actin that concurrently 'slip and grip' (Ponti et al., 2004; Jurado et al., 2005) to facilitate movement by linking highly regulated intracellular flowing actin to the extracellular substrate via transmembrane integrin adhesions (Wiseman et al., 2004; Lawson et al., 2012; Alexandrova et al., 2008; Goult et al., 2013; Changede et al., 2015; Sun et al., 2014). Transient engagement of the actin through adhesions is part of a mechanism that transduces force from flowing actin and is termed the molecular clutch (Chan and Odde, 2008; Hu et al., 2007; Brown et al., 2006; Ishibashi et al., 2015; Chen et al., 2012; Case and Waterman, 2015; Havrylenko et al., 2014). Flowing actin therefore represents a population that is not engaged with adhesions, whereas immobile actin (in the external reference frame) represents a population in contact with adhesions.

With these features in mind, we first investigated cell speed on a population level (thousands of cells measured) in polarised migrating murine effector T-cells exposed to a range of stimuli, all in the presence of an ICAM-1 coating on a glass coverslip. Fig. S1 shows that cells slow down when exposed to $MnCl_2$ or high surface concentrations of ICAM-1, and speed up in the presence of chemokine CXCL12 as well as in cells in which PTPN22 has been genetically deleted. To characterise the dynamics of actin flow in more detail, primary mouse T-cells, expressing a Lifeact–GFP transgene were allowed to migrate on glass surfaces coated with ICAM-1 before being imaged by TIRF microscopy (Fig. 1A). As a proxy for actin linked to the molecular clutch, Fourier analysis was used to determine the fraction of immobile actin in cells, since stationary portions of the actin cytoskeleton must necessarily be engaged with extracellular substrate while the cell migrates over that position. Subsequently, the centre of the cell was continually reset, shifting the frame of reference from the laboratory frame, to the cell frame (Fig. 1B), while spatiotemporal image correlation spectroscopy (STICS) was used to measure the velocity and directionality of flowing (unengaged) actin relative to the cell, that is, from the frame of reference of the cell (Fig. 1C).

For cells migrating on ICAM-1 (2 µg/ml), 75±5% (median ±interquartile range) of pixels contained more than 50% immobile F-actin over 5 s time windows (Fig. 1D). Slower cells, treated with CytoD, Mn^{2+} or a high ICAM concentration (100 µg/ml), displayed a significantly increased percentage of pixels displaying immobile actin ($P<0.0001$; Fig. 1D). In contrast, faster migrating cells (treated with CXCL12 or PTPN22$^{-/-}$ cells) had significantly lower percentages of pixels containing immobile actin ($P<0.0001$).

STICS was then used to analyse the flow speeds of unengaged actin, relative to the cell (Fig. 1E). T-cells migrating on ICAM-1 (2 µg/ml) alone had an average cell speed of 13.19 µm/min (blue), with retrograde flowing actin moving faster at 18.95 µm/min (orange). Conditions that slowed cell migration also slowed actin retrograde flow speed. However, in all cases, actin flow speed remained much higher than cell speed. The percentage values above the bars show that, in slower cells, treated with CytoD, Mn^{2+} or a high concentration of ICAM-1, actin speed was 192%, 239%, and 91% higher than the cell speed, respectively. Adding CXCL12 to cells or measuring PTPN22$^{-/-}$ cells led to faster cell migration which was also coupled to faster actin retrograde flow. Furthermore, Fig. 1F shows that in all conditions, the fraction of pixels in which actin was immobile was inversely correlated to cell speed (r values for correlation shown in table, $P<0.0001$). Therefore, we concluded that decreased actin engagement correlates with increased cell speed. Taken together, these data indicate that retrograde actin flow is always greater than the overall velocity of the T-cell and that the proportion of immobile actin is inversely related to cell speed.

The size and number of LFA-1 membrane nanoclusters increase with T-cell speed

When effector T-cells migrate on ICAM-1-coated glass, they adopt a polarised morphology (Hogg et al., 2004; Comrie et al., 2015; Valignat et al., 2013; Ridley et al., 2003). Previously, studies of integrin affinity have shown a specific pattern where LFA-1 within the LE exists predominantly in the intermediate affinity form, whereas high affinity LFA-1 is detected in the mid cell body/FZ (Smith et al., 2007). It has been reported, in slow moving cells, that integrin-based adhesions change their size as they mature (Kanchanawong et al., 2010). We therefore tested whether T-cells use differential membrane LFA-1 nano-clustering to regulate cell migration.

We investigated integrin LFA-1 nanoscale clustering in conditions that speed up or slow T-cell migration by performing dSTORM and Bayesian cluster analysis (Rubin-Delanchy et al., 2015; Griffié et al., 2016). Effector T-cells were allowed to migrate on ICAM-1-coated glass for 15 min in the presence of conditioned or nonconditioned medium, and these were compared with PTPN22$^{-/-}$ cells. Cells were fixed, surface LFA-1 detected with anti-LFA-1 antibody conjugated to Alexa Fluor 647 (AF647) (clone 2D7), STORM acquisition performed and coordinate pointillist maps generated for Bayesian cluster analysis. Stationary effector T-cells were used as non-polarised T-cell controls (no ICAM-1 on the coverglass). Representative STORM images and cluster maps of a 2×2 µm region of interest (ROI) within a stationary and migrating T-cell are shown (Fig. 2A,B). ROIs from round stationary cells were taken at random, as they do not have a LE and FZ. T-cell velocities were measured for each condition by automatic tracking before fixation for SMLM (as previously shown in Fig. S1).

In polarised T-cells, the FZ displayed different LFA-1 clustering properties to the LE. The number of LFA-1 clusters per ROI was consistently increased in the FZ (Fig. 2C). Compared to the LE, the size of clusters was significantly decreased in the FZ (Fig. 2D), whereas the number of molecules per cluster was significantly increased (Fig. 2E). Together, this represents a median increase in cluster density in FZ clusters (blue bars), compared to LE clusters (orange bars). This is achieved both through a size contraction and an increase in molecular content of the clusters. Compared to stationary cells, clusters in the cell membrane of polarised migrating T-cells increase in number, in size and in molecular content. Together, this indicates that T-cells adopt a regionally discriminated LFA-1 nanoclustering programme to achieve polarised T-cell migration.

Journal of Cell Science (2020) 133, jcs232991. doi:10.1242/jcs.232991

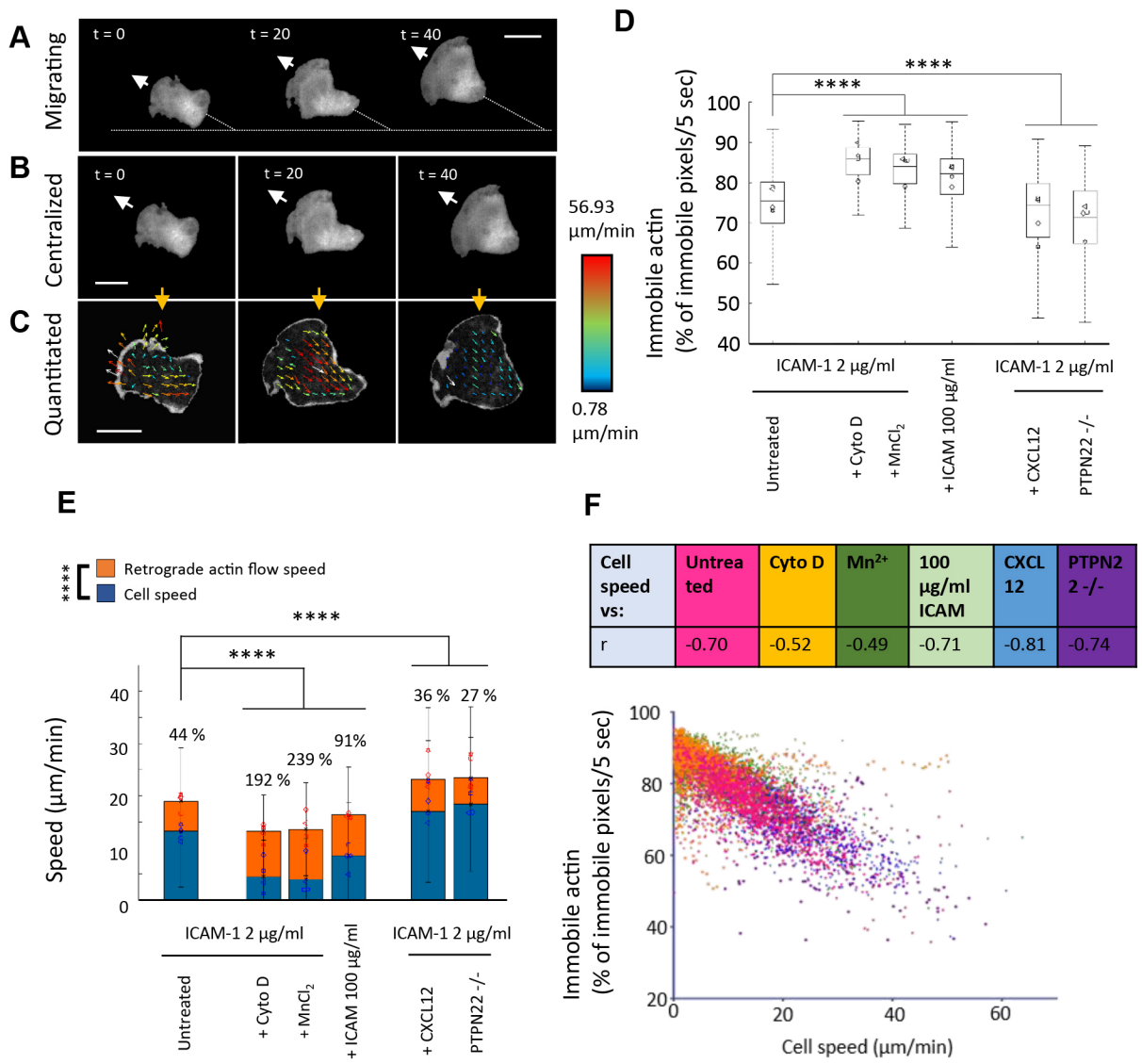

Fig. 1. Fast cells exhibit decreased actin attachment to adhesions and increased flow speed. (A) Example frames from representative TIRF movies of actin in a migrating T-cell. t, time in seconds. Dotted lines illustrate cell movement. Scale bar: 4 µm. (B) The same cell as in A was moved into the centre of the field of view in each frame, in order to change the frame of reference from the microscope (external reference frame) to the cell (internal reference frame), and (C) STICS vector maps from the centralized cell according to the colour map shown on the right. (D) Box plot showing immobile actin as the percentage of immobile pixels in a 5 s window derived from the external reference frame. The box represents the IQR, the line represents the median, and the whiskers show the range for pooled data from the mice. The diamonds represent per mouse median values. (E) Median cell speed (the blue bar depicts pooled median from three mice, blue symbols depict median values from each mouse) and retrograde actin flow speed (orange bars and symbols) from the internal reference frame. (F) Plot showing negative correlation between the percentage of immobile pixels over 5 s versus cell speed: table above shows r values for correlation in each condition. *n*=4 mice, 50 cells per mouse, 200 cells per condition. Kruskal–Wallis testing was used to compare pooled non-parametric data between each condition. ****P<0.0001.

The number of clusters significantly decreased in cells that migrated faster owing to treatment with CXCL12 or lack of PTPN22 (Fig. 2C) as compared to slower cells (Mn^{2+} treated, high ICAM-1 concentration and untreated controls). Slower moving cells had a similar number of LFA-1 nanoclusters to untreated control cells (Fig. 2C). The size of clusters was significantly increased in the LE and FZ of T-cells treated with CXCL12 [32% LE and 22% FZ increase with CXCL12 compared to ICAM-1 alone (P<0.0001)] and PTPN22$^{-/-}$ [33% LE and 23% FZ increase in PTPN22$^{-/-}$ compared to ICAM-1 alone (P<0.0001)] (Fig. 2D). The number of localisations per cluster was increased in faster moving T-cells to a greater extent in the LE than in the FZ [29% LE and 15% FZ increase with CXCL12 compared to ICAM-1 alone (P<0.0001); (24% LE and 5% FZ increase in PTPN22$^{-/-}$ compared to ICAM-1 alone (P<0.0001)] (Fig. 2E).

In slower moving T-cells treated with CytoD or $MnCl_2$, we observed a minor increase in cluster size (<9% LE and FZ), and an intermediate increase of 25% and 17% in the LE and FZ of cells migrating on higher concentrations of ICAM-1 (100 µg/ml), respectively. In CytoD-treated cells, the molecules per cluster increased by 35% and 25% in the LE and FZ, respectively. In $MnCl_2$-treated cells, the molecules per cluster increased by <6%, whereas in cells migrating on an increased concentration of ICAM-1, molecules per cluster was increased by 35% and 15% in the LE and FZ, respectively. Together, this indicates a more substantial increase in cluster size, and a concomitant increase in molecular content

Journal of Cell Science (2020) 133, jcs232991. doi:10.1242/jcs.232991

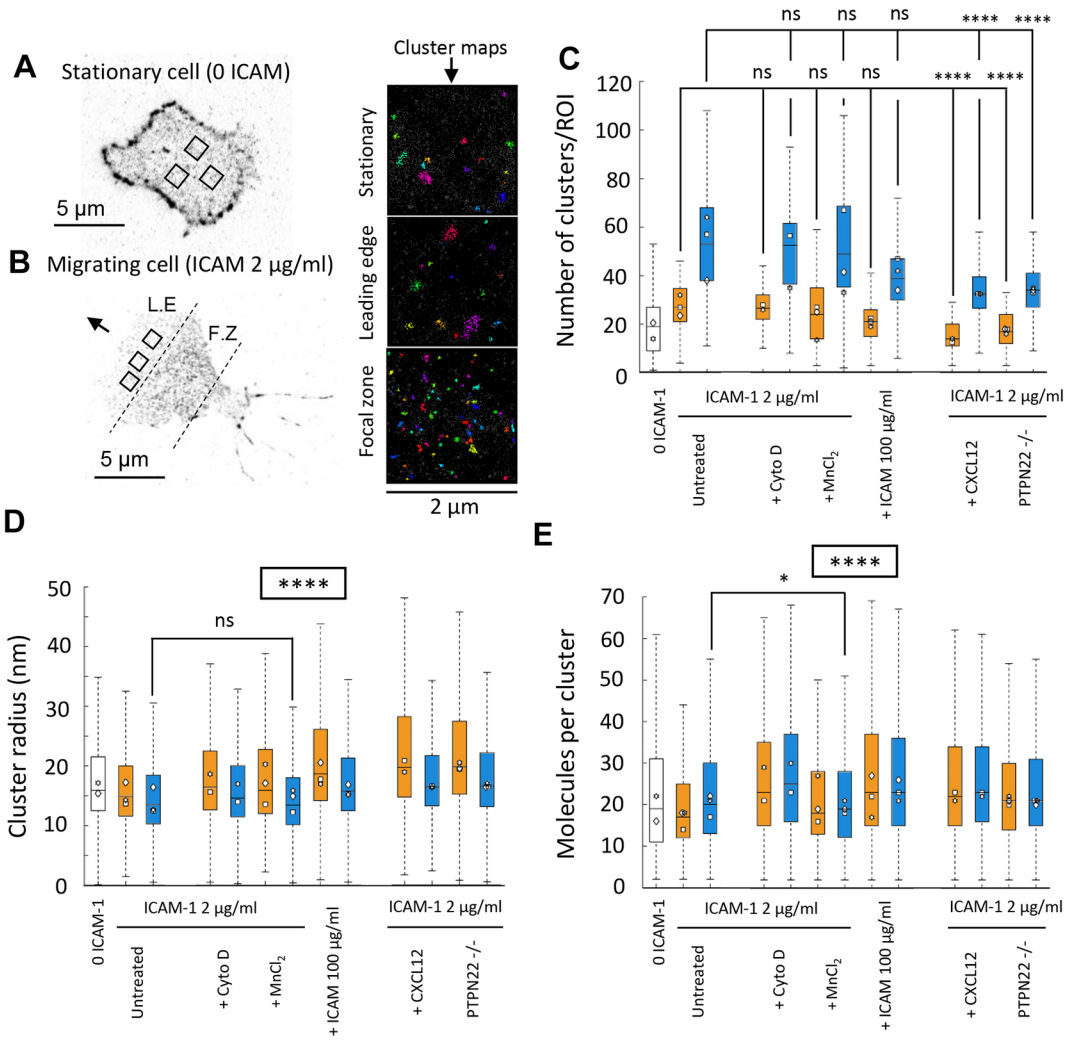

Fig. 2. Integrin LFA-1 membrane nanoclusters increase in density and decrease in number in fast migrating cells. (A,B) Example pointillist maps derived from STORM imaging of LFA-1 in a stationary T-cell (A) and a migrating T-cell (B). Boxes in A and B denote 2 µm^2 regions chosen for analysis and representative cluster maps on the right. (C–E) Metrics for cells in A and B. In each plot, metrics extracted for stationary cells have clear bars, and migrating cells are split up into LE (orange bars) and FZ (blue bars). From left to right conditions are: no (0) ICAM-1; 2 µg/ml ICAM-1-coated coverslip (untreated), 2 µg/ml ICAM-1-coated coverslip with added cytochalasin D, Mn^{2+} or a higher concentration of ICAM-1 (100 µg/ml), then, 2 µg/ml ICAM-1-coated coverslip with CXCL2 added at 150 ng/ml or using PTPN22$^{-/-}$ cells. Metrics extracted consist of (C) number of clusters per ROI, (D) cluster radius (nm) and (E) the molecules per cluster. (n=350 ROIs and 40 cells per condition from three separate mice). Kruskal–Wallis testing was used to compare pooled non-parametric data between each condition. ns, not significant; *P<0.05; ****P<0.0001. The boxed **** in D and E denotes that results were P<0.0001 between every condition, apart from for untreated (FZ) versus $MnCL_2$ (FZ).

(representing maintained cluster density) in fast moving cells. Slow moving cells showed negligible changes in cluster size (Mn^{2+} or CytoD treated). Mn^{2+}-treated clusters had negligible changes to molecular content, whereas CytoD-treated cells experienced an increase in cluster density. All changes were more substantial in the LE compared to the FZ. All changes are summarised in Table S1.

These results suggest that integrin LFA-1 membrane clusters are modulated on the nanoscale and this influences the migration speed of the cell. Clusters adopt a small dense profile in the high affinity integrin-rich FZ, and a larger less dense profile in the reduced affinity LE. Clusters are larger and less dense in faster migrating cells. The data suggest that these zone-specific cluster patterns may be hardwired into polarised T-cells and indicate that the biophysical arrangement of LFA-1 is regulated in conjunction with integrin affinity to control cell speed. As there are fewer clusters in faster moving cells, we next investigated the 3D profile of nanoclusters of LFA-1 to determine whether this phenomenon relates to the recruitment of LFA-1 to the membrane from submembrane stores.

The size of 3D intracellular LFA-1 clusters increases above the FZ as cell speed decreases

LFA-1 is constantly recycled to and from the cell membrane to facilitate cell migration. Accordingly, we investigated whether the intracellular pool of membrane-proximal LFA-1 became nanoclustered, and if so, whether it was similarly zonally distributed to surface LFA-1 and whether that distribution was modulated with cell migration dynamics. Interferometric photoactivatable light microscopy (iPALM) (Shtengel et al., 2009) was used for the acquisition of 3D single-molecule data with ∼20 nm z-precision to a depth of ∼500 nm from the height of the coverslip. The same battery of conditions were used to slow down and speed up migrating T-cells, which were tracked to confirm their speed prior to fixation. Fig. 3A illustrates a representative iPALM z-projection of cytosolic LFA-1 nanoclusters

Journal of Cell Science (2020) 133, jcs232991. doi:10.1242/jcs.232991

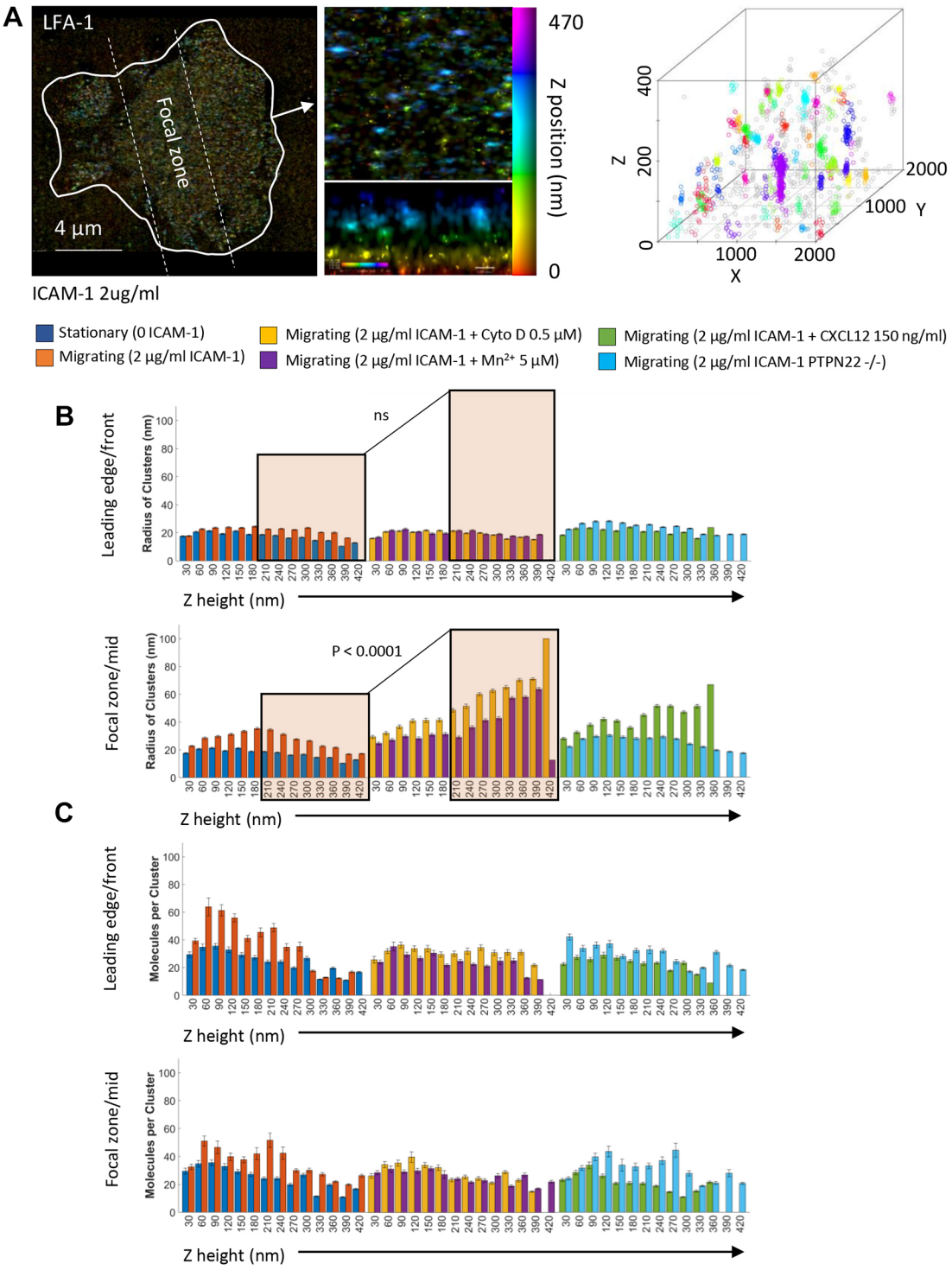

Fig. 3. Intracellular LFA-1 nanoclusters are larger in slow moving cells above the FZ. (A) Representative iPALM *z*-projection of LFA-1 in a migrating T-cell (left panel), zoomed region in *xy* and *xz* side view (middle panel), and arbitrarily coloured clusters identified in a 2000×2000 nm region by Bayesian cluster analysis (right panel). (B,C) The radius of clusters (B) and the molecules per cluster (C) were extracted from the cluster maps for stationary cells (0 ICAM-1) and migrating cells (2 µg/ml ICAM-1) (left hand plots), and CytoD and $MnCl_2$ treated (middle plots), and CXCL12 and PTPN22$^{-/-}$ cells (right plots). The orange shaded areas in B denote larger clusters higher above the membrane in slow cells, which are not present in untreated migrating cells. *n*=3 mice, 20 cells and 200 ROIs per condition. Kruskal–Wallis testing was used to compare pooled data from *z*-heights 0 to 210 nm versus 240 to 420 nm.

in a migrating T-cell (left) and the result of Bayesian 3D cluster analysis (Griffié et al., 2017) in a representative 2000×2000×400 nm ROI (right). Cluster descriptors for the size and number of molecules per cluster were then extracted from ROIs in the FZ or the LE and plotted as a function of the *z*-height from the coverslip.

Clustering in migrating cells was regionally distinct between the LE and FZ. In the LE, clusters in migrating cells compared to stationary cells exhibited almost no increase in size (Fig. 3B, top panel), but this was accompanied by an increase in the number of molecules per cluster (Fig. 3C, top panel; P<0.0001). Clusters in migrating cells also

Journal of Cell Science (2020) 133, jcs232991. doi:10.1242/jcs.232991

exhibited an increase in size, focused at a region 200 nm above the coverslip (Fig. 3B, lower panel; $P<0.0001$). The number of molecules per cluster was also increased in the FZ of migrating cells (Fig. 3C; $P<0.0001$). Together, this indicates that, in the switch from stationary to migrating phenotype, 3D LFA-1 clustering becomes region specific, where clusters above the LE increase in density and clusters above the FZ increase in size and slightly increase their molecular content, concentrated close to the cell membrane.

In cells with a slower migration (treated with CytoD or Mn^{2+}), effects on nanoclusters occur above the FZ, whereas LE clusters remain constant (orange box, top panel Fig. 3B). FZ-specific nanoclusters increase in size, especially in the range 210 to 410 nm above the cell membrane (Fig. 3B, orange box, lower panel; $P<0.0001$), with a similar number of molecules at all z-heights in the range 0 to 420 nm. Thus, intracellular LFA-1 nanoclusters become larger and less dense in cells that migrate slower. In faster migrating PTPN22$^{-/-}$ cells, the size of intracellular LFA-1 nanoclusters remains similar to those in PTPN22$^{+/+}$ cells in both the LE and FZ, with a decrease in the number of molecules per cluster (Fig. 3B,C, orange compared to light blue bars). Activating T-cells with CXCL12 (Fig. 3B, orange compared to green) slightly increased the size of LFA-1 molecules per cluster high above the membrane (z=210 to 420 nm) with an LE focused reduction the in molecules per cluster (Fig. 3D, orange to green). Intracellular LFA-1 clusters in PTPN22$^{-/-}$ fast cells stay the same size and remain the same density, and in CXCL12-treated cells become slightly larger higher up.

Deleting PTPN22 increases T-cell velocity, and the nanoscale colocalisation of pY397 FAK, pY416Src and LFA-1

Integrin-based adhesions are regulated by an array of kinases and phosphatases. Phosphorylation of FAK is a feature of active ICAM-1–LFA-1 signalling (Zhang and Wang, 2012; Sánchez-Mártin et al., 2004), and is implicated in the first stages of nascent adhesion formation in non-leukocytes (Swaminathan et al., 2016). FAK is basally activated by the Src family kinase LCK in effector T-cells at Y576 or Y577 (depending on species), and Y925. This primes FAK for full activation though phosphorylation at the auto-phosphorylation site Y397 (herein denoted pY397 FAK) (Chapman and Houtman, 2014), which in turn regulates LFA-1 adhesion and de-adhesion (Raab et al., 2017). Expression of dominant-negative mutants of FAK in T-cells reduces the speed of migration on ICAM-1-coated glass (Rose et al., 2003), and overexpression of a negative regulator of FAK phosphorylation impairs LFA-1 clustering and reduces ICAM-1–LFA-1-driven T-cell homo-aggregation (Giannoni et al., 2003). PTPN22 is a cytosolic phosphatase that acts with C-terminal Src kinase (CSK) to negatively regulate LCK and ZAP-70 downstream of LFA-1 engagement (Burn et al., 2016). CSK is also regulated by FAK (Chapman and Houtman, 2014). Auto-phosphorylated pY397 FAK has also been described as being associated with active integrin in vesicles above the membrane (Nader et al., 2016; Kleinschmidt and Schlaepfer, 2017).

We therefore employed iPALM and Bayesian cluster analysis to study 3D pY397 FAK localisation in stationary and migrating PTPN22$^{+/+}$ or PTPN22$^{-/-}$ cells. An example pseudocoloured 3D localisation map is shown in Fig. 4A. ROIs were chosen from the cells, and Bayesian cluster analysis carried out to produce cluster maps (Fig. 4B). pY397 FAK staining was verified using FAK inhibitor 14, which blocks Y397 phosphorylation (Fig. S2). ROIs from the LE or FZ regions were quantified in terms of their radius and molecules per cluster as a function of the z-height (Fig. 4C,D).

When comparing stationary cells to cells migrating on ICAM-1, pY397 FAK cluster size (Fig. 4C) was largely unchanged above the LE and FZ, in both PTPN22$^{+/+}$ and PTPN22$^{-/-}$ cells. The number of molecules per cluster was higher close to the cell membrane (z=0 to 210 nm) in the LE and FZ, meaning that such clusters retained their size but increased in density (Fig. 4D). The size of and number of molecules per cluster was similar between stationary cells and that seen in the LE of migrating cells. Clusters became less dense (of similar size but with fewer molecules per cluster) close to the membrane in the FZ of migrating cells (Fig. 4D, blue shaded box, z=0 to 210 nm; $P<0.0001$).

PTPN22$^{-/-}$ stationary cells (no ICAM-1) adopted pY397 FAK nanoclusters high above the membrane (orange box in Fig. 4C, comparing blue versus orange bars at z=270 to 390 nm; $P<0.0001$), which were not present in PTPN22$^{+/+}$ cells. This population of high clusters present in PTPN22$^{-/-}$ stationary cells has the same number of molecules per cluster as those lower down in z-height, representing a maintenance of density (Fig. 4D). During migration, lack of PTPN22 did not change the size or density of intracellular pY397 FAK clusters.

As nanoclusters resemble nascent adhesions in non-leukocytes, but occur throughout the cell, we next investigated how they are regulated in T-cells. We tested whether the lack of PTPN22 causes changes in the colocalisation of pFAK with LFA-1 and a second set of signalling intermediates, the Src family kinases, using multi-colour SMLM microscopy (Yi et al., 2016, 2017). Wild-type or PTPN22$^{-/-}$ primary murine T-cell blasts were plated on ICAM-1, allowed to migrate and tracked by live-cell imaging. They were then fixed, stained and imaged using madSTORM (Yi et al., 2016), permitting the sequential imaging of pY397 FAK, Src family kinases phosphorylated at pY416 (denoted pY416 Src) and LFA-1. Fig. S3 shows the overall cell speeds, where PTPN22$^{-/-}$ cells were faster than PTPN22$^{+/+}$ cells directly prior to fixation. Fig. 5A shows a representative cell post fixation after three rounds of sequential staining and imaging.

In wild-type migrating T-cells, LFA-1, pY397 FAK and pY416 Src clusters co-existed on a similar size scale and with similar numbers of molecules per cluster (Fig. 5B,C). LFA-1, pY397 FAK and pY416 Src clusters were consistently larger with more molecules in the LE compared to the FZ. PTPN22$^{-/-}$ cells displayed significantly larger clusters of all three species in both the LE and FZ, combined with significantly more molecules per cluster. PTPN22 deficiency therefore increases the clustering of all three proteins, but especially pY397 FAK and pY416 Src family kinases. Extraction of Pearson's correlation coefficients (PCCs) for the colocalisation of clusters of each species showed that LFA-1 clusters were more colocalised with pY397 FAK clusters when PTPN22 was not present (Fig. 5D). pY397 FAK was also more colocalised with pY416 Src family kinases in PTPN22$^{-/-}$ cells (Fig. 5E). The colocalisation of LFA-1 clusters with pY416 Src family kinase clusters was unchanged (Fig. 5F). Taken together, faster migrating PTPN22$^{-/-}$ cells display larger LFA-1, pFAK and pSrc clusters, which are more often colocalised spatially at the nanoscale. The increase in the number of molecules per cluster in the case of pY416 Src family kinases and pY397 FAK supports existing literature describing the action of PTPN22 on LCK, a well characterised participant in early integrin adhesion signalling that itself upregulates FAK phosphorylation (Chapman and Houtman, 2014). Additionally, we do not believe that the absence of PTPN22 is compensated for by upregulation of any other phosphatase activity, as the data show a clear increase in total phosphorylation of

Journal of Cell Science (2020) 133, jcs232991. doi:10.1242/jcs.232991

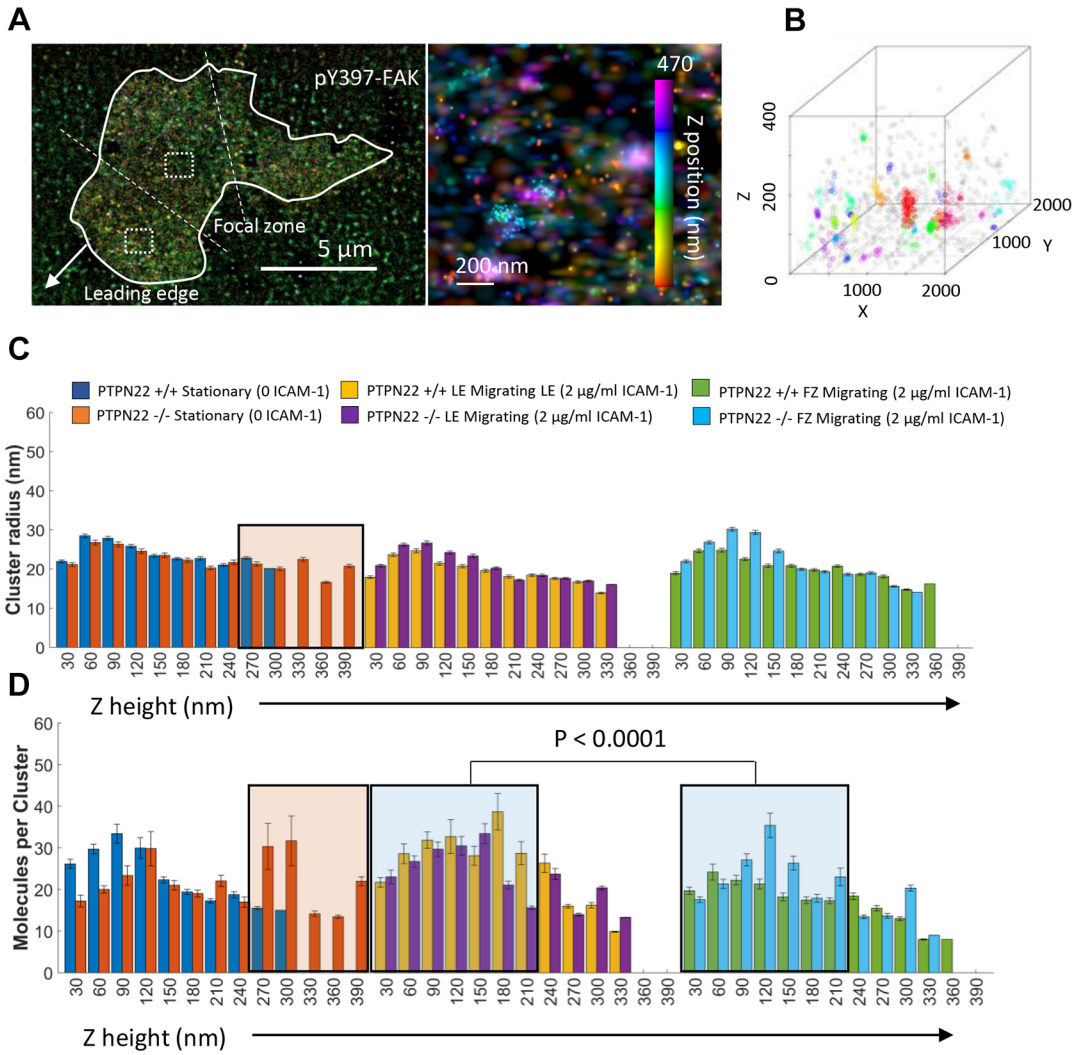

Fig. 4. Intracellular 3D pY397 FAK nanoclusters are of similar size and density in migrating and stationary cells, while deleting PTPN22 increases membrane distal pools of pY397 FAK. (A) An example pseudocoloured cluster map of pY397 FAK nanoclusters in a migrating T-cell (direction of migration indicated by white arrow) (left) is shown alongside a zoomed image where clusters can be visualised at different height scales from 0 to 470 nm (right panel with *z* colour bar). (B) An example cluster map with defined 3D clusters. For the radius of clusters (C) and the number of molecules per cluster (D), the leftmost plots show stationary PTPN22$^{+/+}$ or PTPN22$^{-/-}$ cells (0 ICAM-1), the middle plots show the LE of migrating PTPN22$^{+/+}$ and PTPN22$^{-/-}$ cells (2 µg/ml ICAM-1) and the right-hand plots show the FZ of migrating PTPN22$^{+/+}$ and PTPN22$^{-/-}$ cells (2 µg/ml ICAM-1). *n*=3 mice, 20 cells and 200 ROIs per condition. Error bars denote s.e.m. Orange shaded areas denote the population of clusters present in PTPN22$^{-/-}$ cells and not in PTPN22$^{+/+}$ cells. Blue shaded areas denote a reduction in the density of clusters in the FZ compared to the LE, close to the membrane. Kruskal–Wallis testing was used to compare pooled data from *z*-heights 0 to 210 nm versus 240 to 420 nm.

direct (Src family kinases) and indirect (FAK) PTPN22 substrates in PTPN22$^{-/-}$ cells (Fig. S4).

DISCUSSION

We employed advanced and super-resolved imaging methods to study the nanoscale migration machinery in T-cells. Specifically, we quantified the nanoscale distribution of membrane-localised and intracellular LFA-1 alongside actin flow dynamics in migrating T-cells to understand the relationship between integrin affinity-clustering and engagement with flowing actin and the speed of T-cell propulsion. Our data indicate that: (1) actin flow and engagement drive migration, where engagement is inversely correlated to cell speed, and the flow rate of unengaged actin is positively correlated; (2) T-cells exploit differential clustering of hundreds of tiny nano-adhesions to translate force from the actin cytoskeleton to the substrate; (3) LFA-1 and pY397 FAK nano-adhesions adopt region-specific clustering patterns both in 2D in the membrane and in 3D above the membrane; (4) changes to cell speed induced by a battery of signals modulate adhesion nano-cluster size and density; and (5) the deletion of PTPN22 phosphatase causes faster T-cell migration, and modulates LFA-1 and pY397 FAK clustering in 2D and 3D. Importantly, lack of this phosphatase induced an increase in colocalization of LFA-1, pY397-Src family kinase and pY416-FAK in nanoclusters, coupled to an actin flow speed increase, actin engagement decrease and cell migration speed increase (summarised in Fig. 6).

The front (LE)/middle (FZ) trends in LFA-1 (2D and 3D), pY397 FAK (2D and 3D) and pY416 Src (2D) indicated here are characterised for the first time. For LFA-1, reported trends for affinity occur in the same zones: high affinity integrin occurs in the FZ, whereas low/intermediate affinity integrin predominates in the LE (Persson et al., 2018; Evans et al., 2011; Smith et al.,

Journal of Cell Science (2020) 133, jcs232991. doi:10.1242/jcs.232991

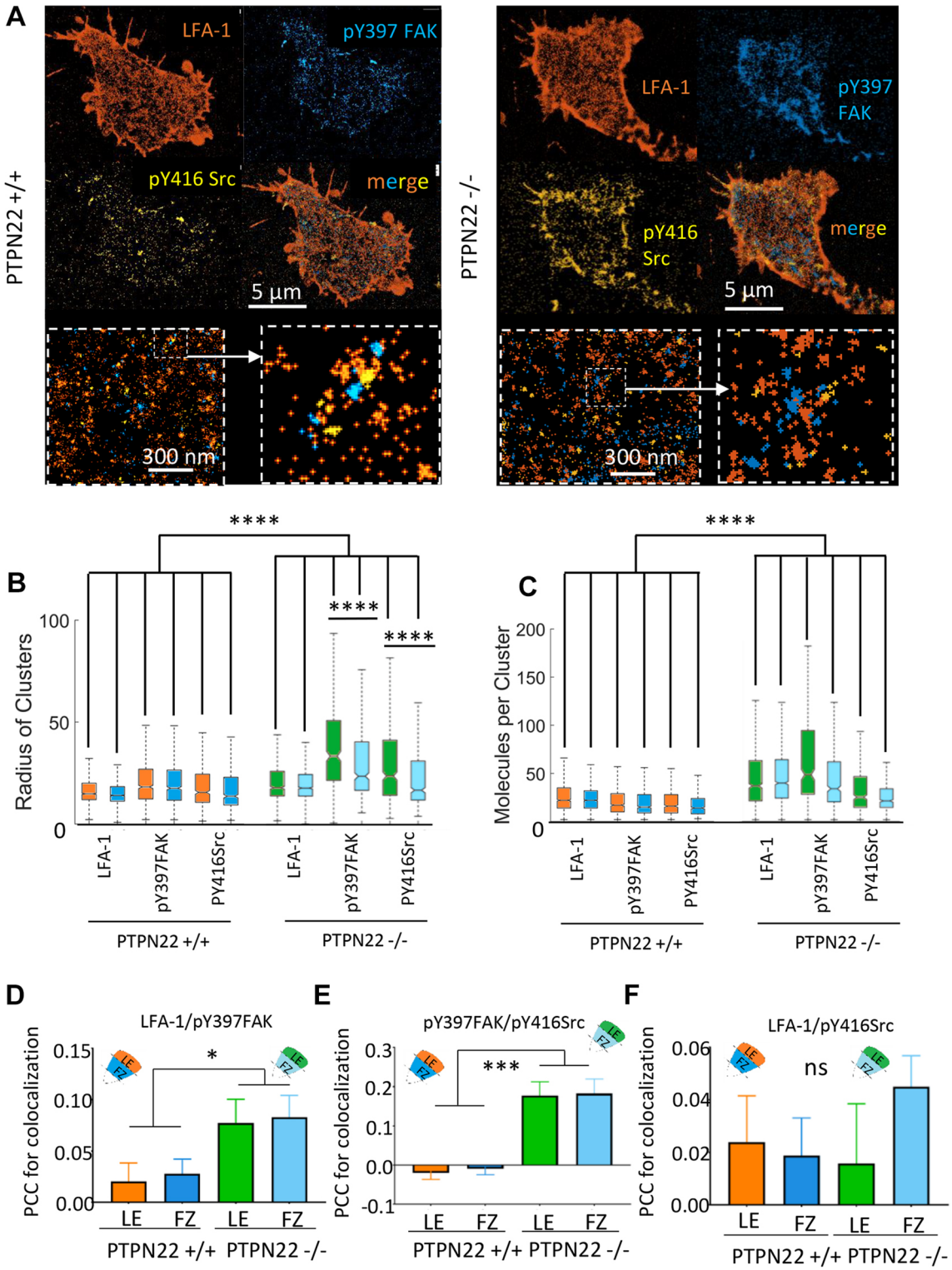

Fig. 5. Cluster size and number of molecules per cluster increase in faster moving PTPN22$^{-/-}$ cells in the cases of LFA-1, pY397 FAK and pY416 Src, which show a higher degree of colocalisation. Individual cells were sequentially stained and imaged by madSTORM; LFA-1, pY397 FAK and pY416 Src family kinases in the same cell are shown (A). LFA-1 clusters are larger (B) and denser (C) in faster moving PTPN22$^{-/-}$ cells compared to slower moving PTPN22$^{+/+}$ cells. pY397 FAK and pY416 Src clusters are also larger and denser in PTPN22$^{-/-}$ cells. The size of pY397 FAK and pY416 Src clusters in PTPN22$^{-/-}$ are more strongly regionally discriminated: (A) clusters in the LE are larger than those in the FZ, though the molecular content stays the same. (D–F) Pearson's correlation coefficient for cluster colocalisation. (D) LFA-1 colocalised with pY397 FAK to a higher level in PTPN22$^{-/-}$ cells than in PTPN22$^{+/+}$ cells, and (E) pY397 FAK colocalised more with pY416 Src in PTPN22$^{-/-}$ cells PTPN22$^{+/+}$ cells. (F) LFA-1 and pY416 Src displayed similar levels of colocalisation in PTPN22$^{+/+}$ and PTPN22$^{-/-}$ cells. n=21 PTPN22$^{+/+}$ cells and 13 PTPN22$^{-/-}$ cells. *P<0.05, **P<0.01, ***P<0.001, ****P<0.0001. The box represents the 25–75th percentiles, and the median is indicated with the line. The whiskers show the complete range. Error bars in D–F denote s.e.m. Kruskal–Wallis and Dunn's post hoc testing was used to compare the clustering of each molecule, in each zone, in PTPN22$^{+/+}$ or PTPN22$^{-/-}$ cells.

Journal of Cell Science (2020) 133, jcs232991. doi:10.1242/jcs.232991

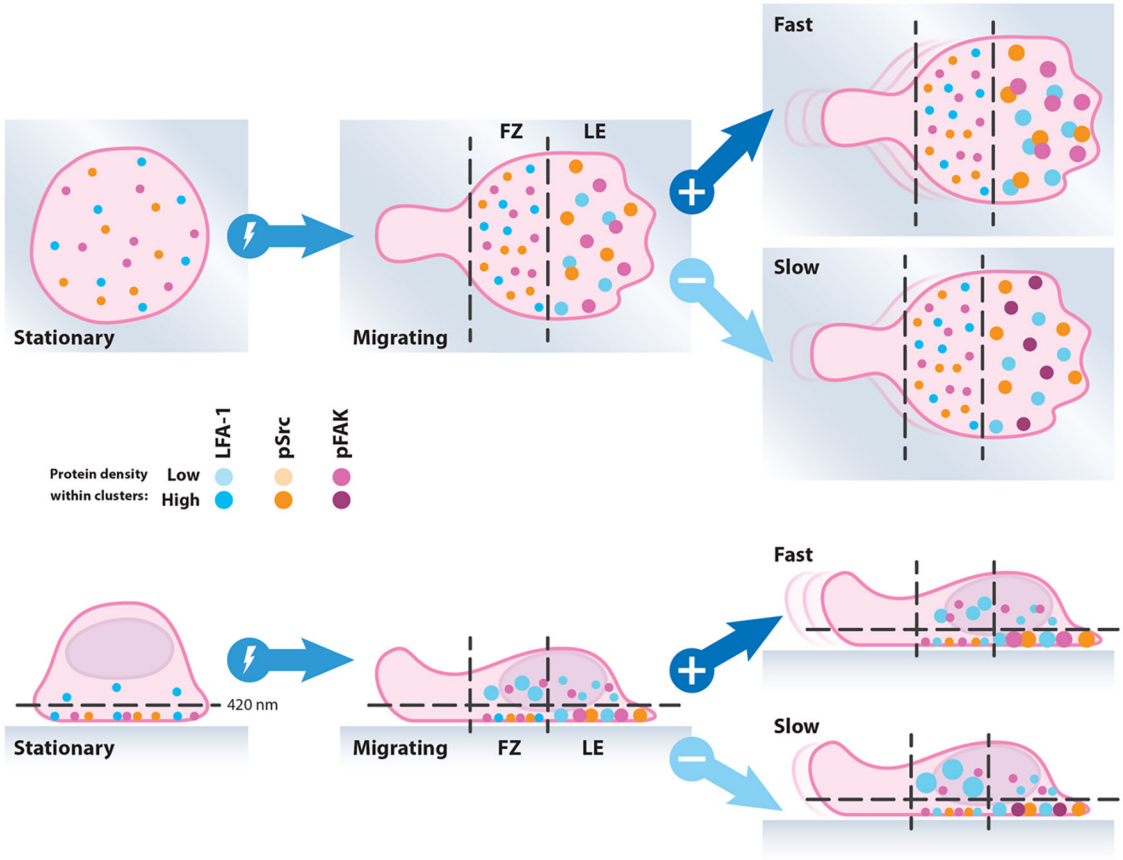

Fig. 6. Schematic diagram of integrin nanoclustering in migrating T-cells. There is greater clustering of surface adhesion molecules at the front of migrating cells, which become larger and more colocalised when those cells migrate rapidly. In contrast, a pool of large adhesion molecule clusters exists intracellularly above the FZ, which become larger for slow moving cells.

2005). In addition, nano-adhesions here differ from adhesions in slower moving cells, which are founded as 'nascent adhesions' and grow as they mature into larger multi-molecular clutch assemblies towards the middle of the cell. The data here indicate a different system, where high affinity LFA-1 adopts smaller, denser and more numerous cluster arrays in the FZ. Intracellular LFA-1 clusters are larger above the FZ, and intracellular pY397 FAK clusters are denser above the LE. Coupled with the actin work, this indicates that these clusters provide an area of increased adhesion in the FZ; it may be that this adhesion imbalance between the LE and FZ enables fast forward cell migration.

In conditions that increase cell speed, nano-adhesions become larger and are joined by larger clusters of phosphorylated kinases (pY397 FAK and pY416 Src family kinases). The integration of multiple molecules into the same nanocluster may necessitate its increase in size in this way. That this effect is also seen in cells knocked out for PTPN22, which directly targets LCK, a Src family kinase that itself phosphorylates FAK, indicates that the size, density and number of LFA-1 clusters is modulated by such kinases and phosphatases on the nanoscale. Pools of intracellular LFA-1 decrease in density in rapidly migrating cells, and intracellular pY397 FAK clusters stay the same size, indicating a further level of control of adhesion based on the nature of LFA-1 undergoing recycling.

It is also important to note that T-cells are capable of several modes of migration, depending on their environmental niche. Here, we study ICAM-1–LFA-1-dependent migration, coupled to actin treadmilling and engagement. High speed polarised T-cell crawling is a phenomenon that occurs in the lymphatic capillaries, during lymph node entry, tissue entry and fast dendritic cell (DC) scanning by T-cells (Teijeira et al., 2017). Such integrin-dependent migration is especially important during inflammation, including in autoimmune disease (Teijeira et al., 2017), and is a physiological requirement for high speed migration (Hons et al., 2018). Integrin-free slower migration relies mainly on RhoGTPase-mediated actin remodelling and predominates in the dense, fibrous interstitium (ICAM-1 blockade does not affect cell migration in this location). In the lymph nodes, both integrin-independent and integrin-dependent fast migration occur, where ICAM-1 blockade reduces T-cell migration speed considerably. *In vitro*, the presence of ICAM-1 potentiates migration speed by 50 to 30% in confined 3D (under agarose; Hons et al., 2018), although in such a system the cells do not require integrin to migrate slowly. Previously, the simple unconfined ICAM-1-coated glass system used here has been used to characterise integrin affinity states (Persson et al., 2018; Evans et al., 2011). Here, we used it to characterise the contribution of nanoclustering and its effect on actin engagement and cell speed.

Overall, we demonstrate that T-cells use individually regulated integrin-based, kinase/phosphatase-coupled 'nano-adhesions' to achieve fast migration. Such nano-adhesions are similar to previously described nascent adhesions (Sun et al., 2014) in size and molecular composition, but differ in that they are regulated on a sub-diffraction length scale throughout the cell membrane, and not only in the LE. The differential inclusion of proxy markers for integrin activity (phosphorylated FAK and Src family kinases) indicates the highly spatial nature of such adhesion regulation (summarised in Fig. 6). We posit that this nano-adhesion system, as

Journal of Cell Science (2020) 133, jcs232991. doi:10.1242/jcs.232991

opposed to a classical adhesion system, with maturation from nascent adhesions to focal complexes and then focal adhesions, represents a novel way for T-cells to quickly turn over individual adhesions to achieve dynamic feats of migration depending on external or internal cues. Our results agree with the conventional understanding of how integrins associate with the actin treadmill as a 'molecular clutch' to facilitate adhesive traction, with the important difference being that T-cells utilise nanoscale 'clutches' of LFA-1 adhesive units that are at least 100-fold reduced in size and polarised in their cellular location. We suggest that these features potentiate the speed and agility of T-cell migration.

Determining what are the live-cell dynamics and rare events that occur in the regulation of nanoclusters will be key to understanding how cells use spatiotemporal molecular organisation to change their behaviour. New high-throughput techniques (Holden et al., 2014; Gunkel et al., 2014; Yasui et al., 2018) to low-power imaging (Chen et al., 2014) and new fluorescent proteins (Zhang et al., 2016; Chang et al., 2012; Tiwari et al., 2015) may soon enable these kind of investigations, and will be especially important in connecting nanoscale regulation to whole-cell function in diverse settings (Shannon and Owen, 2019), including in autoimmune disease.

MATERIALS AND METHODS

Mice colonies

Mice were bred and maintained in the Biological Services Unit of King's College London in compliance with UK Home Office regulations and local ethically approved guidelines. *Ptpn22*$^{-/-}$ mice maintenance and breeding have been described elsewhere (Clarke et al., 2017; Sanchez-Blanco et al., 2018). Male *β-actinCre/+*; *Lifeact-mEGFP/Y* C57BL6 males were a gift from the laboratory of Dr Karen Liu (Centre for Craniofacial and Regenerative Biology, King's College London, UK), which were crossed with *Ptpn22*$^{-/-}$ C57BL6 females; offspring were backcrossed to generate *Ptpn22*$^{+/+}$ *β-actinCre+*; *Lifeact-mEGFP*$^{+}$ and *Ptpn22*$^{-/-}$ *β-actinCre+*; *Lifeact-mEGFP+* males for experiments. Tail blood was genotyped for EGFP expression by flow cytometry. Single-cell suspensions of mouse lymph nodes were stimulated with 1 µg/ml of concanavalin A. After 48 h, T-blasts were re-suspended in medium supplemented with 20 ng/ml human recombinant IL-2 (Proleukin) for an additional 3 to 5 days before being used for migration assays.

Primary murine T-cell culture

Single-cell suspensions were made from lymph nodes harvested from *Ptpn22*$^{+/+}$, *Ptpn22*$^{-/-}$, and *Ptpn22*$^{+/+}$ *Lifeact-mEGFP EGFP*$^{+}$; *Ptpn22*$^{-/-}$ *EGFP*$^{+}$ mice and stimulated with 1 µg/ml of concanavalin A (Sigma-Aldrich, L7647) at 3×10^6 cells/ml for 48 h in complete medium (RPMI 1640-Glutamax, 10% FBS; penicillin, streptomycin, 100 µM sodium pyruvate, 20 mM Hepes and 20 µM 2-mercaptoethanol). After 48 h, T-blasts were washed and re-suspended at 1×10^6 to 2×10^6 cells/ml in complete medium constantly supplemented with 20 ng/ml human recombinant IL-2 for an additional 3 to 5 days before being used in migration assays.

T-cell migration assay

Migration medium was RPMI 1640-Glutamax, 100 µM sodium pyruvate, 25 mM Hepes, 20 µM 2-mercaptoethanol; 2 µg/ml human recombinant IL-2; equilibrated overnight at 37°C 5% CO_2. Ibidi µ-Slide eight-well glass bottom chamber slides of #1.5H thickness were coated with 2 µg/ml murine recombinant ICAM-1-Fc (R&D systems 796-IC-050) for 1.5 h at 37C. Conditioned migration medium was made by adding supplements [150 ng/ml CXCL12 (Peprotech 250-20A-10), 5 µM $MnCl_2$ (Sigma M1787) and 0.5 µM CytoD (Sigma-Aldrich, C2618)] to cells in migration medium for 10 min prior to addition of 2×10^5 T-cells to ICAM-1-coated slide chambers.

Wide-field live-cell phase-contrast time-lapse microscopy and automatic tracking

Imaging was performed using a Nikon Eclipse TI-e microscope. 200,000 T-cells were plated onto slide chambers, transferred to a pre-warmed microscope chamber and settled for 5 to 10 min before acquisition of time-lapse videos at 37°C in 5% CO_2 under a 10× objective for 15 min (50 ms exposure; 25 s between frames). Automatic tracking to quantify T-cell migration was performed using a custom ICY modular program. Image files were imported in the ND2 format with attached metadata to the ICY interface and cell tracking data was then exported to Graphpad Prism or MATLAB for statistical analysis.

Analysis of actin engagement and flow

The analysis windows or 'time of interest' (TOI) for actin flow and engagement was five frames. Immobile actin was calculated in the external reference frame of the cell by taking the zero component of the temporal Fourier transform. A threshold of 50% was applied to each pixel for it to be counted as immobile. For STICS, we adapted a stationary cell programme (Wilson and Theriot, 2006), which keeps the cell centroid in the centre of the ROI. Actin flow analysis was then carried out using STICS (Hebert et al., 2005).

Fixation and labelling for STORM

Migrating T-cells were fixed using 3% PFA plus 0.1% glutaraldehyde in 80 mM kPIPES, 2 mM $MgCl_2$, EGTA 0.5 mM and 2 mM sucrose at pH 6.8 for 10 min followed by 3%-PFA+0.1% glutaraldehyde in Borax 100 mM for 10 min. Slides were washed once with PBS between each treatment.

For immunofluorescence, T-cells were quenched for auto-fluorescence with 1 mM $NaBH_4$ for 15 min, 0.1 M L-glycine for 15 min, blocked with 10% normal goat serum (Thermo Fisher Scientific, 50062Z) for 30 min at room temperature then stained with primary directly conjugated antibody at a 1:100 dilution in 0.1% BSA for 1.5 h at room temperature.

Antibodies used were anti-mouse CD11a (LFA-1) 2D7 clone (1:1000, Biolegend, UK, 101002), ABfinity rabbit monoclonal anti-pTyr397-FAK clone 31H5L17 (1:1000, Thermo Fisher Scientific, 700255) and rabbit monoclonal anti-pY416-Src clone D49G4 (1:1000, Cell Signaling Technology, 6943BF) antibody. Immunofluorescence validation profiles for these antibodies are available at the company websites upon entering the product codes.

STORM and iPALM

Fixed and stained cells were placed in an oxygen scavenging buffer comprised of three parts, which were stored separately. Part A was comprised of 4 mM Tris (2-carboxyethyl) phosphine hydrochloride (Sigma 51805-45-9), 50% glycerol (Sigma 56-81-5), 25 mM KCl (Sigma 7447-40-7), 20 mM Tris-HCl (Sigma 1185-53-1), 20 µg/ml catalase (Sigma 9001-5-2) and 1 mg/ml glucose oxidase (Sigma G2133) all at pH 7.5, made up to a total volume of 5 ml and stored in aliquots of 50 µl at –20°C. Part B contained 100 mg/ml glucose and 10% glycerol and in practice was made to a total volume of 40 ml and stored in aliquots of 400 µl volume at –20°C. Part C contained 1 M Cysteamine-HCl, and in practice was made up directly prior to imaging to 1 ml volume. For imaging, an aliquot of each of Part A and Part B was thawed and added to 100 µl of freshly made Part C, supplemented with 450 µl PBS to a total volume of 1 ml. Imaging was performed on a Nikon N-STORM microscope using a Nikon Plan Apo 100× 1.49 NA oil immersion TIRF objective. Cells were imaged under TIRF illumination with a 15 mW 647 nm laser with the 405 nm laser set to maintain photo-blinking and transition to the triplet state by gradually increasing its power from 0.1 to 1 mW. Emitted fluorescence was collected at wavelengths above 660 nm, with EM gain 300 on an Andor iXon EM-CCD camera at room temperature. Acquisition time was for ∼2.5 min; 10,000 frames were collected at 10 ms exposure time per frame and pixel size was 160 nm. Molecular coordinates were calculated using ThunderSTORM localisation software (Ovesný et al., 2014) with multi-emitter fitting analysis (Huang et al., 2011) enabled. Cluster analysis was performed using Bayesian analysis in 2D (Rubin-Delanchy et al., 2015; Griffié et al., 2016) or 3D (Griffié et al., 2017). Cluster analysis software is available for download as described in the articles listed above. For iPALM, custom gold nanorod fiducial embedded coverslips (Moore et al., 2018) were coated with ICAM-1. iPALM imaging was performed at the Advanced Imaging Centre at Janelia Research Campus including a Nikon 60× 1.49 Apo TIRF Objective, 647 nm excitation and 405 nm activation and 50 ms exposure time. *x*, *y* and *z* coordinates were derived using custom Peakselector

localisation software, which is available upon request. It is important to note that clustering patterns in the first 60 nm of iPALM data closely matched those in the TIRF data. While detection efficiencies were different between the two techniques, reliable TIRF data closely matched iPALM data at the coverslip.

Single-cell correlative live tracking and multicolour dSTORM by multiplexed madSTORM

T-cells were first tracked during migration. Cells were fixed, and their positions were recorded, and then multiplexed antibody madSTORM, using fiducial nanodiamonds for image alignment (Yi et al., 2016, 2017), was used to achieve multicolour imaging. Three-colour pointillist maps were analysed channel per channel with Bayesian cluster analysis (Griffié et al., 2016), and colocalisation was analysed (Rossy et al., 2014).

Statistics

D'Agostino and Pearson tests were used to check for normality in pooled data (from three or four mice in each condition, where LE and FZ measurements were treated as separate conditions). Kruskal–Wallis testing and Dunn's post hoc testing was used to compare pooled, non-normal data between each condition. All statistical analyses were performed with Graphpad Prism software. It is important to note that due to high numbers of clusters being tested in the case of the radius and molecules per cluster, statistical testing gave very low *P*-values between conditions, therefore these results are also discussed in terms of percentage changes. For multiple comparisons between conditions, one-way analysis of variance (ANOVA) and Kruskal–Wallis testing was used. All statistical analyses were performed with Graphpad Prism software.

Acknowledgements

PTPN22-knockout mice were a kind gift of Rose Zamoyska. Nanodiamonds were a kind gift of Keir Neumann, NIH. Male β-*actinCreER/+; Lifeact-mEGFP/Y* mice were a gift from Dr Karen Liu. We acknowledge use of the Nikon Imaging Centre (NIC), King's College London. For the STICS code and support, we acknowledge Paul W. Wiseman and Elvis Pandzic (McGill University), with cell stationarity code written by Laurence Yolland and Brian Stramer (King's College London). iPALM imaging was done in collaboration with the Advanced Imaging Center at Janelia Research Campus, a facility jointly supported by the Gordon and Betty Moore Foundation, and the Howard Hughes Medical Institute.

Competing interests

The authors declare no competing or financial interests.

Author contributions

Conceptualization: A.P.C.; Methodology: M.J.S.; Software: J.G., J.A., D.J.W., D.M.O.; Validation: M.J.S.; Formal analysis: M.J.S., J.P., J.G.; Investigation: M.J.S.; Resources: J.A., T.P., D.J.W., R.Z.; Writing - original draft: M.J.S., A.P.C., G.H.C., D.M.O.; Writing - review & editing: A.P.C., G.H.C., D.M.O.; Supervision: A.P.C., G.H.C., D.M.O.; Project administration: D.M.O.; Funding acquisition: D.M.O.

Funding

This work was supported by a European Research Council Starter Grant #337187, and Arthritis Research UK Programme grant 20525. M.J.S. was supported by the King's College London Bioscience Institute and the Guy's and St Thomas' Charity Prize PhD Programme in Biomedical and Translational Science.

Supplementary information

Supplementary information available online at
http://jcs.biologists.org/lookup/doi/10.1242/jcs.232991.supplemental

References

Alexandrova, A. Y., Arnold, K., Schaub, S., Vasiliev, J. M., Meister, J.-J., Bershadsky, A. D. and Verkhovsky, A. B. (2008). Comparative dynamics of retrograde actin flow and focal adhesions: formation of nascent adhesions triggers transition from fast to slow flow. *PLoS ONE* **3**, e3234. doi:10.1371/journal.pone.0003234

Begovich, A. B., Carlton, V. E. H., Honigberg, L. A., Schrodi, S. J., Chokkalingam, A. P., Alexander, H. C., Ardlie, K. G., Huang, Q., Smith, A. M., Spoerke, J. M. et al. (2004). A missense single-nucleotide polymorphism in a gene encoding a protein tyrosine phosphatase (PTPN22) is associated with rheumatoid arthritis. *Am. J. Hum. Genet.* **75**, 330-337. doi:10.1086/422827

Bottini, N., Vang, T., Cucca, F. and Mustelin, T. (2006). Role of PTPN22 in type 1 diabetes and other autoimmune diseases. *Semin. Immunol.* **18**, 207-213. doi:10.1016/j.smim.2006.03.008

Brand, O., Gough, S. and Heward, J. (2005). HLA. CTLA-4 and PTPN22: the shared genetic master-key to autoimmunity? *Expert Rev. Mol. Med.* **7**, 1-15. doi:10.1017/S1462399405009981

Brown, C. M., Hebert, B., Kolin, D. L., Zareno, J., Whitmore, L., Horwitz, A. R. and Wiseman, P. W. (2006). Probing the integrin-actin linkage using high-resolution protein velocity mapping. *J. Cell Sci.* **119**, 5204-5214. doi:10.1242/jcs.03321

Burn, G. L., Svensson, L., Sanchez-Blanco, C., Saini, M. and Cope, A. P. (2011). Why is PTPN22 a good candidate susceptibility gene for autoimmune disease? *FEBS Lett.* **585**, 3689-3698. doi:10.1016/j.febslet.2011.04.032

Burn, G. L., Cornish, G. H., Potrzebowska, K., Samuelsson, M., Griffie, J., Minoughan, S., Yates, M., Ashdown, G., Pernodet, N., Morrison, V. L. et al. (2016). Superresolution imaging of the cytoplasmic phosphatase PTPN22 links integrin-mediated T cell adhesion with autoimmunity. *Sci. Signal.* **9**, ra99. doi:10.1126/scisignal.aaf2195

Case, L. B. and Waterman, C. M. (2015). Integration of actin dynamics and cell adhesion by a three-dimensional, mechanosensitive molecular clutch. *Nat. Cell Biol.* **17**, 955-963. doi:10.1038/ncb3191

Chan, C. E. and Odde, D. J. (2008). Traction dynamics of filopodia on compliant substrates. *Science* **322**, 1687-1691. doi:10.1126/science.1163595

Chang, H., Zhang, M., Ji, W., Chen, J., Zhang, Y., Liu, B., Lu, J., Zhang, J., Xu, P. and Xu, T. (2012). A unique series of reversibly switchable fluorescent proteins with beneficial properties for various applications. *Proc. Natl. Acad. Sci. USA* **109**, 4455-4460. doi:10.1073/pnas.1113770109

Changede, R., Xu, X., Margadant, F. and Sheetz, M. P. (2015). Nascent integrin adhesions form on all matrix rigidities after integrin activation. *Dev. Cell* **35**, 614-621. doi:10.1016/j.devcel.2015.11.001

Chapman, N. M. and Houtman, J. C. D. (2014). Functions of the FAK family kinases in T cells: beyond actin cytoskeletal rearrangement. *Immunol. Res.* **59**, 23-34. doi:10.1007/s12026-014-8527-y

Chen, L., Vicente-Manzanares, M., Potvin-Trottier, L., Wiseman, P. W. and Horwitz, A. R. (2012). The integrin-ligand interaction regulates adhesion and migration through a molecular clutch. *PLoS ONE* **7**, e40202. doi:10.1371/journal.pone.0040202

Chen, B.-C., Legant, W. R., Wang, K., Shao, L., Milkie, D. E., Davidson, M. W., Janetopoulos, C., Wu, X. S., Hammer, J. A., Liu, Z. et al. (2014). Lattice light-sheet microscopy: Imaging molecules to embryos at high spatiotemporal resolution. *Science* **346**, 1257998. doi:10.1126/science.1257998

Clarke, F., Jordan, C. K., Gutiérrez-Martinez, E., Bibby, J. A., Sanchez-Blanco, C., Cornish, G. H., Dai, X., Rawlings, D. J., Zamoyska, R. et al. (2017). Protein tyrosine phosphatase PTPN22 is dispensable for dendritic cell antigen processing and promotion of T-cell activation by dendritic cells. *PloS One* **12**, e0186625. doi:10.1371/journal.pone.0186625

Comrie, W. A., Babich, A. and Burkhardt, J. K. (2015). F-actin flow drives affinity maturation and spatial organization of LFA-1 at the immunological synapse. *J. Cell Biol.* **208**, 475-491. doi:10.1083/jcb.201406121

Dai, X., James, R. G., Habib, T., Singh, S., Jackson, S., Khim, S., Moon, R. T., Liggitt, D., Wolf-Yadlin, A., Buckner, J. H. et al. (2013). A disease-associated PTPN22 variant promotes systemic autoimmunity in murine models. *J. Clin. Investig.* **123**, 2024-2036. doi:10.1172/JCI66963

Dransfield, I., Cabañas, C., Craig, A. and Hogg, N. (1992). Divalent cation regulation of the function of the leukocyte integrin LFA-1. *J. Cell Biol.* **116**, 219-226. doi:10.1083/jcb.116.1.219

Evans, R., Lellouch, A. C., Svensson, L., McDowall, A. and Hogg, N. (2011). The integrin LFA-1 signals through ZAP-70 to regulate expression of high-affinity LFA-1 on T lymphocytes. *Blood* **117**, 3331-3342. doi:10.1182/blood-2010-06-289140

Giannoni, E., Chiarugi, P., Cozzi, G., Magnelli, L., Taddei, M. L., Fiaschi, T., Buricchi, F., Raugei, G. and Ramponi, G. (2003). Lymphocyte function-associated antigen-1-mediated T cell adhesion is impaired by low molecular weight phosphotyrosine phosphatase-dependent inhibition of FAK activity. *J. Biol. Chem.* **278**, 36763-36776. doi:10.1074/jbc.M302686200

Goddette, D. W. and Frieden, C. (1986). Actin polymerization. The mechanism of action of cytochalasin D. *J. Biol. Chem.* **261**, 15974-15980.

Goult, B. T. Zacharchenko, T., Bate, N., Tsang, R., Hey, F., Gingras, A. R., Elliott, P. R., Roberts, G. C. K., Ballestrem, C., Critchley, D. R. et al. (2013). RIAM and vinculin binding to talin are mutually exclusive and regulate adhesion assembly and turnover. *J. Biol. Chem.* **288**, 8238-8249. doi:10.1074/jbc.M112.438119

Griffié, J., Shannon, M., Bromley, C. L., Boelen, L., Burn, G. L., Williamson, D. J., Heard, N. A., Cope, A. P., Owen, D. M. and Rubin-Delanchy, P. (2016). A Bayesian cluster analysis method for single-molecule localization microscopy data. *Nat. Protoc.* **11**, 2499-2514. doi:10.1038/nprot.2016.149

Griffié, J., Shlomovich, L., Williamson, D. J., Shannon, M., Aaron, J., Khuon, S., L. Burn, G., Boelen, L., Peters, R., Cope, A. P. et al. (2017). 3D Bayesian cluster analysis of super-resolution data reveals LAT recruitment to the T cell synapse. *Sci. Rep.* **7**, 4077. doi:10.1038/s41598-017-04450-w

Gunkel, M., Flottmann, B., Heilemann, M., Reymann, J. and Erfle, H. (2014). Integrated and correlative high-throughput and super-resolution microscopy. *Histochem. Cell Biol.* **141**, 597-603. doi:10.1007/s00418-014-1209-y

Havrylenko, S., Mezanges, X., Batchelder, E. and Plastino, J. (2014). Extending the molecular clutch beyond actin-based cell motility. *New J. Phys.* **16**, 105012. doi:10.1088/1367-2630/16/10/105012

Hebert, B., Costantino, S. and Wiseman, P. W. (2005). Spatiotemporal image correlation spectroscopy (STICS) theory, verification, and application to protein velocity mapping in living CHO cells. *Biophys. J.* **88**, 3601-3614. doi:10.1529/biophysj.104.054874

Hogg, N. (2004). How T cells use LFA-1 to attach and migrate. *Immunol. Lett.* **92**, 51-54. doi:10.1016/j.imlet.2003.10.014

Holden, S. J., Pengo, T., Meibom, K. L., Fernandez Fernandez, C., Collier, J. and Manley, S. (2014). High throughput 3D super-resolution microscopy reveals Caulobacter crescentus in vivo Z-ring organization. *Proc. Natl. Acad. Sci. USA* **111**, 4566-4571. doi:10.1073/pnas.1313368111

Hons, M., Kopf, A., Hauschild, R., Leithner, A., Gaertner, F., Abe, J., Renkawitz, J., Stein, J. V. and Sixt, M. (2018). Chemokines and integrins independently tune actin flow and substrate friction during intranodal migration of T cells. *Nat. Immunol.* **19**, 606-616. doi:10.1038/s41590-018-0109-z

Hu, K. Ji, L., Applegate, K. T., Danuser, G. and Waterman-Storer, C. M. (2007). Differential transmission of actin motion within focal adhesions. *Science* **315**, 111-115. doi:10.1126/science.1135085

Huang, F., Schwartz, S. L., Byars, J. M. and Lidke, K. A. (2011). Simultaneous multiple-emitter fitting for single molecule super-resolution imaging. *Biomed. Opt. Express* **2**, 1377-1393. doi:10.1364/BOE.2.001377

Ishibashi, M., Miyanaga, Y., Matsuoka, S., Kozuka, J., Togashi, Y., Kinashi, T. and Ueda, M. (2015). Integrin LFA-1 regulates cell adhesion via transient clutch formation. *Biochem. Biophys. Res. Commun.* **464**, 459-466. doi:10.1016/j.bbrc.2015.06.155

Jurado, C., Haserick, J. R. and Lee, J. (2005). Slipping or gripping? Fluorescent speckle microscopy in fish keratocytes reveals two different mechanisms for generating a retrograde flow of actin. *Mol. Biol. Cell* **16**, 507-518. doi:10.1091/mbc.e04-10-0860

Kanchanawong, P., Shtengel, G., Pasapera, A. M., Ramko, E. B., Davidson, M. W., Hess, H. F. and Waterman, C. M. (2010). Nanoscale architecture of integrin-based cell adhesions. *Nature* **468**, 580-584. doi:10.1038/nature09621

Kleinschmidt, E. G. and Schlaepfer, D. D. (2017). Focal adhesion kinase signaling in unexpected places. *Curr. Opin. Cell Biol.* **45**, 24-30. doi:10.1016/j.ceb.2017.01.003

Lawson, C., Lim, S.-T., Uryu, S., Chen, X. L., Calderwood, D. A. and Schlaepfer, D. D. (2012). FAK promotes recruitment of talin to nascent adhesions to control cell motility. *J. Cell Biol.* **196**, 223-232. doi:10.1083/jcb.201108078

Moore, T. I., Aaron, J., Chew, T.-L. and Springer, T. A. (2018). Measuring integrin conformational change on the cell surface with super-resolution microscopy. *Cell Reports* **22**, 1903-1912. doi:10.1016/j.celrep.2018.01.062

Nader, G. P. F., Ezratty, E. J. and Gundersen, G. G. (2016). FAK, talin and PIPKIγ regulate endocytosed integrin activation to polarize focal adhesion assembly. *Nat. Cell Biol.* **18**, 491-503. doi:10.1038/ncb3333

Nordenfelt, P., Elliott, H. L. and Springer, T. A. (2016). Coordinated integrin activation by actin-dependent force during T-cell migration. *Nat. Commun.* **7**, 13119. doi:10.1038/ncomms13119

Ovesný, M., Křížek, P., Borkovec, J., Švindrych, Z. and Hagen, G. M. (2014). ThunderSTORM: a comprehensive ImageJ plug-in for PALM and STORM data analysis and super-resolution imaging. *Bioinformatics* **30**, 2389-2390. doi:10.1093/bioinformatics/btu202

Persson, H., Potrzebowski, W., Potrzebowska, K. and Svensson, L. M. (2018). Spatial mapping of affinity changes for the integrin LFA-1 during cell migration using clusters identified based on local density. *J. Biophotonics* **12**, e201800080. doi:10.1002/jbio.201800080

Ponti, A., Machacek, M., Gupton, S. L., Waterman-Storer, C. M. and Danuser, G. (2004). Two distinct actin networks drive the protrusion of migrating cells. *Science* **305**, 1782-1786. doi:10.1126/science.1100533

Raab, M., Lu, Y., Kohler, K., Smith, X., Strebhardt, K. and Rudd, C. E. (2017). LFA-1 activates focal adhesion kinases FAK1/PYK2 to generate LAT-GRB2-SKAP1 complexes that terminate T-cell conjugate formation. *Nat. Commun.* **8**, 16001. doi:10.1038/ncomms16001

Ridley, A. J., Schwartz, M. A., Burridge, K., Firtel, R. A., Ginsberg, M. H., Borisy, G., Parsons, J. T. and Horwitz, A. R. (2003). Cell migration: integrating signals from front to back. *Science* **302**. doi:10.1126/science.1092053

Rose, D. M., Liu, S., Woodside, D. G., Han, J., Schlaepfer, D. D. and Ginsberg, M. H. (2003). Paxillin binding to the 4 integrin subunit stimulates LFA-1 (Integrin L 2)-dependent T cell migration by augmenting the activation of focal adhesion kinase/proline-rich tyrosine kinase-2. *J. Immunol.* **170**, 5912-5918. doi:10.4049/jimmunol.170.12.5912

Rossy, J., Cohen, E., Gaus, K. and Owen, D. M. (2014). Method for co-cluster analysis in multichannel single-molecule localisation data. *Histochem. Cell Biol.* **141**, 605-612. doi:10.1007/s00418-014-1208-z

Rubin-Delanchy, P., Burn, G. L., Griffié, J., Williamson, D. J., Heard, N. A., Cope, A. P. and Owen, D. M. (2015). Bayesian cluster identification in single-molecule localization microscopy data. *Nat. Methods* **12**, 1072-1076. doi:10.1038/nmeth.3612

Rust, M. J., Bates, M. and Zhuang, X. (2006). Sub-diffraction-limit imaging by stochastic optical reconstruction microscopy (STORM). *Nat. Methods* **3**, 793-796. doi:10.1038/nmeth929

Sanchez-Blanco, C., Clarke, F., Cornish, G. H., Depoil, D., Thompson, S. J., Dai, X., Rawlings, D. J., Dustin, M.L., Zamoyska, R., Cope, A. P. and Purvis, H. A. et al. (2018). Protein tyrosine phosphatase PTPN22 regulates LFA-1 dependent Th1 responses. *J. Autoimmun.* **94**, 45-55. doi:10.1016/j.jaut.2018.07.008

Sánchez-Mártin, L., Sánchez-Sánchez, N., Gutiérrez-López, M. D., Rojo, A. I., Vicente-Manzanares, M., Pérez-Alvarez, M. J., Sánchez-Mateos, P., Bustelo, X. R., Cuadrado, A., Sánchez-Madrid, F. et al. (2004). Signaling through the leukocyte integrin LFA-1 in T cells induces a transient activation of Rac-1 that is regulated by Vav and PI3K/Akt-1. *J. Biol. Chem.* **279**, 16194-16205. doi:10.1074/jbc.M400905200

Shannon, M. and Owen, D. M. (2019). Bridging the nanoscopy-immunology gap. *Front. Phys.* **6**, 157. doi:10.3389/fphy.2018.00157

Shannon, M. J., Burn, G., Cope, A., Cornish, G. and Owen, D. M. (2015). Protein clustering and spatial organization in T-cells. *Biochem. Soc. Trans.* **43**, 315-321. doi:10.1042/BST20140316

Shtengel, G., Galbraith, J. A., Galbraith, C. G., Lippincott-Schwartz, J., Gillette, J. M., Manley, S., Sougrat, R., Waterman, C. M., Kanchanawong, P., Davidson, M. W. et al. (2009). Interferometric fluorescent super-resolution microscopy resolves 3D cellular ultrastructure. *Proc. Natl. Acad. Sci. USA* **106**, 3125-3130. doi:10.1073/pnas.0813131106

Smith, A., Carrasco, Y. R., Stanley, P., Kieffer, N., Batista, F. D. and Hogg, N. (2005). A talin-dependent LFA-1 focal zone is formed by rapidly migrating T lymphocytes. *J. Cell Biol.* **170**, 141-151. doi:10.1083/jcb.200412032

Smith, A., Stanley, P., Jones, K., Svensson, L., Mcdowall, A. and Hogg, N. (2007). The role of the integrin LFA-1 in T-lymphocyte migration. *Immunol. Rev.* **218**, 135-146. doi:10.1111/j.1600-065X.2007.00537.x

Sun, Z., Lambacher, A. and Fässler, R., (2014). Nascent adhesions: from fluctuations to a hierarchical organization. *Curr. Biol.* **24**, R801-R803. doi:10.1016/j.cub.2014.07.061

Svensson, L., Burn, G., Sanchez-Blanco, C., Zamoyska, R. and Cope, A. (2011). Lyp/PTPN22 is a negative regulator of integrin mediated T cell adhesion and migration; the disease associated PTPN22 allelic variant is a loss of function mutant that perturbs T cell migration. *Ann. Rheum. Dis.* **70**, A7. doi:10.1136/ard.2010.149096.16

Swaminathan, V., Fischer, R. S. and Waterman, C. M. (2016). The FAK-Arp2/3 interaction promotes leading edge advance and haptosensing by coupling nascent adhesions to lamellipodia actin. *Mol. Biol. Cell* **27**, 1085-1100. doi:10.1091/mbc.E15-08-0590

Teijeira, A., Hunter, M. C., Russo, E., Proulx, S. T., Frei, T., Debes, G. F., Coles, M., Melero, I., Detmar, M., Rouzaut, A. et al. (2017). T cell migration from inflamed skin to draining lymph nodes requires intralymphatic crawling supported by ICAM-1/LFA-1 interactions. *Cell Reports* **18**, 857-865. doi:10.1016/j.celrep.2016.12.078

Tiwari, D. K., Arai, Y., Yamanaka, M., Matsuda, T., Agetsuma, M., Nakano, M., Fujita, K. and Nagai, T. (2015). A fast- and positively photoswitchable fluorescent protein for ultralow-laser-power RESOLFT nanoscopy. *Nat. Methods* **12**, 515-518. doi:10.1038/nmeth.3362

Valignat, M.-P., Theodoly, O., Gucciardi, A., Hogg, N. and Lellouch, A. C. (2013). T lymphocytes orient against the direction of fluid flow during LFA-1-mediated migration. *Biophys. J.* **104**, 322-331. doi:10.1016/j.bpj.2012.12.007

Wilson, C. A. and Theriot, J. A. (2006). A correlation-based approach to calculate rotation and translation of moving cells. *IEEE Trans. Image Process.* **15**, 1939-1951. doi:10.1109/TIP.2006.873434

Wiseman, P. W., Brown, C. M., Webb, D. J., Hebert, B., Johnson, N. L., Squier, J. A., Ellisman, M. H. and Horwitz, A. F. (2004). Spatial mapping of integrin interactions and dynamics during cell migration by image correlation microscopy. *J. Cell Sci.* **117**, 5521-5534. doi:10.1242/jcs.01416

Yasui, M., Hiroshima, M., Kozuka, J., Sako, Y. and Ueda, M. (2018). Automated single-molecule imaging in living cells. *Nat. Commun.* **9**, 3061. doi:10.1038/s41467-018-05524-7

Yi, J., Manna, A., Barr, V. A., Hong, J., Neuman, K. C. and Samelson, L. E. (2017). Highly multiplexed, super-resolution imaging of T cells using madSTORM. *J. Vis. Exp.* **124**, e55997. doi:10.3791/55997

Yi, J. Manna, A., Barr, V. A., Hong, J., Neuman, K. C. and Lippincott-Schwartz, J. (2016). madSTORM: a superresolution technique for large-scale multiplexing at single-molecule accuracy. *Mol. Biol. Cell* **27**, 3591-3600. doi:10.1091/mbc.e16-05-0330

Zhang, Y. and Wang, H. (2012). Integrin signalling and function in immune cells. *Immunology* **135**, 268-275. doi:10.1111/j.1365-2567.2011.03549.x

Zhang, X., Zhang, M., Li, D., He, W., Peng, J., Betzig, E. and Xu, P. (2016). Highly photostable, reversibly photoswitchable fluorescent protein with high contrast ratio for live-cell superresolution microscopy. *Proc. Natl. Acad. Sci. USA* **113**, 10364-10369. doi:10.1073/pnas.1611038113